DPNU – 88 – 15
SLAC – PUB – 4489
April 28, 1988
M

SPIN-PARITY DETERMINATION OF THE $\phi_J(1850)$ FROM K^-p INTERACTIONS AT 11 GEV/C*

D. ASTON,[1] N. AWAJI,[2a] T. BIENZ,[1] F. BIRD,[1] J. D'AMORE,[3]
W. DUNWOODIE,[1] R. ENDORF,[3] K. FUJII,[2b] H. HAYASHII,[2c] S. IWATA,[2b]
W.B. JOHNSON,[1] R. KAJIKAWA,[2] P. KUNZ,[1] D.W.G.S. LEITH,[1] L. LEVINSON,[1d]
T. MATSUI,[2b] B.T. MEADOWS,[3] A. MIYAMOTO,[2b] M. NUSSBAUM,[3] H. OZAKI,[2]
C.O. PAK,[2b] B.N. RATCLIFF,[1] D. SCHULTZ,[1] S. SHAPIRO,[1] T. SHIMOMURA,[2e]
P. K. SINERVO,[1f] A. SUGIYAMA,[2] S. SUZUKI,[2] G. TARNOPOLSKY,[1g]
T. TAUCHI,[2b] N. TOGE,[1] K. UKAI,[4] A. WAITE,[1h] S. WILLIAMS[1i]

[1] *Stanford Linear Accelerator Center, Stanford University, P.O. Box 4349, Stanford, California 94305, U.S.A.*
[2] *Department of Physics, Nagoya University, Furo-cho, Chikusa-ku, Nagoya 464, Japan*
[3] *University of Cincinnati, Cincinnati, Ohio 45221, U.S.A.*
[4] *Institute for Nuclear Study, University of Tokyo, Midori-cho, Tanashi, Tokyo 188, Japan*

ABSTRACT

High statistics data from the reactions $K^-p \to K^-K^+\Lambda$ and $K^-p \to K^0_S K^\pm\pi^\mp\Lambda$ at 11 GeV/c have been obtained in the LASS spectrometer at SLAC. Spherical harmonic moment and amplitude analyses of the K^-K^+ system confirm the existence of the $\phi_J(1850)$ and demonstrate that its quantum numbers are $I^G(J^{PC}) = 0^-(3^{--})$. Evidence for a $K^*\overline{K}(+c.c.)$ decay mode is also presented.

Submitted to *Physics Letters B*

* Work supported in part by the Department of Energy under contract No. DE-AC03-76SF00515; the National Science Foundation under grant Nos. PHY82-09144, PHY85-13808, and the Japan U.S. Cooperative Research Project on High Energy Physics.

Present Addresses :
a Fujitsu Limited, Nakahara-ku, Kawasaki 211, Japan.
b National Laboratory for High Energy Physics, KEK, Oho-machi, Tsukuba, Ibaraki 305, Japan.
c Nara Women's University, Kitauoya-nishi-machi, Nara-shi, Nara 630, Japan.
d Weismann Institute, Rehovot 76100, Israel.
e Nippon BIO-RAD Laboratories, 1-2-7 Shiba-Daimon, Minato-ku, Tokyo 105, Japan.
f University of Pennsylvania, Philadelphia, Pennsylvania 19104, U.S.A.
g Hewlett-Packard Laboratories, 1501 Page Mill Road, Palo Alto, California 94304, U.S.A.
h Department of Physics, University of Victoria, Victoria BC, Canada V8W 2Y2
i Diasonics Corp., 533 Cabot Rd., S. San Francisco, CA 94090, U.S.A.

The excitations of the $s\bar{s}$ (strangeonium) system are poorly understood. In particular, only the two lowest mass orbital excitations, the $\phi(1020)$ and the $f'_2(1525)$, are well measured. Evidence for a candidate $J^P = 3^-$ state at ~ 1850 MeV/c^2 has been presented [1, 2], but the spin-parity assignment is uncertain. The neutral $K\overline{K}$ system produced by a kaon beam is ideal for the study of natural spin-parity strangeonia. The peripheral production of such a system is dominated by hypercharge exchange (K and K^* exchange), and experiments have shown that the resulting low-mass $K\overline{K}$ spectrum consists primarily of strangeonium states [3]. However, in order to investigate such states with mass ~ 2 GeV/c^2 a kaon beam of at least 6 GeV/c is required. At such energies, the relevant final states have small cross sections, so that large exposures are necessary. It follows that the number of experiments which can meaningfully attempt an understanding of these states is rather limited.

In this paper, we present results of an analysis of the K^-K^+ system in the $\phi_J(1850)$ region and compare them with results on $K^0_S K^\pm\pi^\mp$ final states from the same experiment [4]. These systems are produced in the reactions

$$K^-p \to K^-K^+\Lambda_{seen}, \tag{1}$$

$$K^-p \to K^0_S K^\pm\pi^\mp\Lambda_{seen} \tag{2}$$

at 11 GeV/c. All final state particles, including those from the decay of the recoil Λ, are measured in the spectrometer, so that the data samples are very clean.

The data were obtained with the Large Aperture Superconducting Solenoid (LASS) spectrometer at SLAC, the details of which are described elsewhere [3-6]. The useful beam flux corresponds to a sensitivity of 4.1 events/nb, and the acceptance is approximately isotropic over almost the full 4π solid angle. After event reconstruction, events from reaction (1) which have $t' \leq 1.0$ (GeV/c)^2 ($t' \equiv |t| - |t|_{min}$, where t is the momentum transfer squared from target proton to Λ) are selected to enhance the dominant

hypercharge exchange processes. Contamination in this sample from the final states $\pi^+\pi^-\Lambda$ and $p\bar{p}\Lambda$ is negligibly small, while the Σ^0 background is estimated at $\sim 8\%$. The final data sample contains 12,294 events.

Figs. 1a-b show the corresponding Dalitz plot and K^-K^+ invariant mass distribution, respectively. The well-known $\phi(1020)$ and $f_2'(1525)$ dominate the K^-K^+ mass spectrum, and there is evidence of structure in the $f_2(1270)/a_2(1320)$ region. At higher mass, a faint band of events can be seen in fig. 1a at ~ 1.8 GeV/c^2, which projects to the small, but significant, peak in the range 1.8 - 1.9 GeV/c^2 of fig. 1b. The Dalitz plot shows substantial diffractive production of $N^* \rightarrow K^+\Lambda$. This appears to become significant for K^-K^+ mass above ~ 1.7 GeV/c^2, and to dominate the region above 2.0 GeV/c^2.

The invariant K^-K^+ mass distribution of fig. 1b may be compared to the summed $K^0_S K^\pm \pi^\mp$ distribution from reactions (2) [4], which is shown in fig. 1c. The latter exhibits a sharp rise at $K^*\overline{K}$ threshold, followed by peaks at ~ 1.5 and ~ 1.85 GeV/c^2, close to the positions of the $f_2'(1525)$ and the $\phi_J(1850)$, respectively. Caution must be exercised in relating these peaks to the corresponding signals in fig. 1b, since several states are expected in each of these mass regions. Indeed, a partial wave analysis of reactions (2) in this experiment [4] has shown that the peak at ~ 1.5 GeV/c^2 is due to the $J^P = 1^+$ amplitude, rather than the $f_2'(1525)$, which dominates the $K\overline{K}$ spectrum at this mass. Moreover, the peak in the $\phi_J(1850)$ region results predominantly from the production of $J^P = 2^-$ and 1^+ amplitudes. However, in addition to these large unnatural spin-parity contributions, which cannot occur in reaction (1), $\sim 25\%$ of the intensity at ~ 1.85 GeV/c^2 was found to result from the production of a natural spin-parity 3^- amplitude. This will be discussed further below.

The K^-K^+ helicity amplitude structure in the $\phi_J(1850)$ region for reaction (1) can be extracted from the mass dependence of the K^-K^+ angular distribution in the t-

channel helicity frame. To this end, the data in the mass interval 1.68 - 2.04 GeV/c^2 are divided into low t' ($t' \leq 0.2$ (GeV/c)^2; 575 events) and high t' ($0.2 \leq t' \leq 1.0$ (GeV/c)^2; 780 events) samples, which are analysed separately. The low t' region is expected to be dominated by helicity zero amplitudes produced by unnatural parity exchange, whereas in the high t' region the main contributions should be due to helicity one amplitudes produced by natural parity exchange.

The acceptance corrected spherical harmonic moments ($t_{LM} = \sqrt{4\pi} N \langle Y_{LM} \rangle; L \leq 8, M = 0$) in the t-channel helicity frame are shown in fig. 2 for the $\phi_J(1850)$ region. It should be noted that amplitudes with spin J can contribute to moments with L up to $2J$.

For the low t' data, there is a peak in the mass spectrum, t_{00}, at ~ 1.86 GeV/c^2, and similar structure appears for all moments with $L \leq 6$. No such structure is observed in the corresponding even L moments for the $K^0_S K^0_S$ system produced in the reaction $K^-p \rightarrow K^0_S K^0_S \Lambda_{recn}$ in the present experiment [6], indicating that the effect is associated with a state having odd angular momentum, viz. J=3,5,..*etc.* Since moments with $L \geq 7$ exhibit no signal in the $\phi_J(1850)$ region for reaction (1) (cf. fig. 2), we conclude that a $J^P = 3^-$ object exists in this mass region, and is responsible for the peaks observed in the low t' data of figs. 2a-g. The solid curve of fig. 2a results from a fit of a quadratic background plus a relativistic F-wave Breit-Wigner (B-W) form to the low t' data. The fit yields mass and width estimates for the $\phi_3(1850)$ of 1855 ± 10 MeV/c^2 and 64 ± 31 MeV/c^2, respectively.

For the high t' data of fig. 2, t_{00} again shows an excess of events at ~ 1.86 GeV/c^2. The dashed curve is the result of a fit using the same functional form as at low t', but with mass and width parameters fixed at 1855 and 64 MeV/c^2, respectively. The fit is reasonable, and indicates that the signal at high t' is approximately half that at low t'. Of the remaining moments, t_{10}, t_{20}, and t_{30} show no structure whereas t_{40}, t_{50}, and

t_{60} exhibit a dip rather than a peak at $\sim$ 1.86 GeV/c^2; a dip is also observed for t_{70}, while t_{80} is consistent with zero, as at low t'. In order to understand the differences between the low t' and high t' moments, we must consider how the moments relate to the underlying helicity amplitudes.

The spherical harmonic moments can be expressed as bilinear products of production amplitudes $L_{\lambda\pm}$ of the K^-K^+ system with spin L and t-channel helicity λ, via natural (+) or unnatural (−) parity exchange [7]. Since the measured moments with $M > 2$ are consistent with zero, amplitudes with $\lambda > 1$ can be neglected and all moments up to $L = 6$, $M = 2$ expressed in terms of the amplitudes S_0, P_0, $P_\pm$, D_0, $D_\pm$, F_0 and $F_\pm$, where we have adopted the simplified notation, $L_0 \equiv L_{0-}$, and $L_\pm \equiv L_{1\pm}$.

In the $\phi_3(1850)$ region all low t' moments up to t_{60} exhibit a peak. In order to investigate the underlying amplitude structure, linear combinations of the t_{LM} are created such that the resulting amplitude products contain one term involving F_0, the additional terms depending on S, P and D amplitudes only. The results, labelled according to F_0 term, are shown in figs. 3a-d.

Peaks are observed at $\sim$ 1.86 GeV/c^2 in all four low t' distributions. At high t', fig. 3a shows no structure, whereas the others appear to dip at $\sim$ 1.86 GeV/c^2. Since the line-shape due to the imaginary part of a narrow B-W amplitude is very similar to that due to the modulus squared, the peak in the low t' data of figs. 3a-c may result in each case from interference between an F_0 B-W amplitude and an approximately imaginary background. Fits using the imaginary part of a B-W plus a linear background yield average mass and width estimates for the $\phi_3(1850)$ of 1858 ± 12 MeV/c^2 and 58 ± 36 MeV/c^2, respectively, and the curves of figs. 3a-c correspond to these values. These results agree well with those from the mass projection, t_{00}, even though the interference terms represented by figs. 3a-c make no contribution to this

quantity, which depends upon only the modulus squared of each amplitude.

This result implies that the S_0, P_0 and D_0 amplitudes add approximately coherently with relative strength given by the peak heights of figs. 3a-c to form a background amplitude at low t' which is almost purely imaginary. An amplitude describing diffractive production of a low mass ΛK^+ system in reaction (1) would be expected to have such properties. To test this hypothesis, the low t' K^-K^+ mass spectrum in the $\phi_3(1850)$ region is plotted in fig. 4a for events with ΛK^+ mass below (solid dots) and above (open dots) 2.2 GeV/c^2. The high mass data show a broad maximum, while the low mass data show a very sharp peak similar to those observed in figs. 3a-c. Indeed, the curve in fig. 4a corresponds to a fit using the imaginary part of a B-W which yields mass and width 1856 ± 9 MeV/c^2 and 54 ± 28 MeV/c^2, respectively, in good agreement with the results from figs. 3a-c. The low t' distribution in $\cos\theta_{GJ}$ for the peak bin (1.84 - 1.88 GeV/c^2) is shown in fig. 4c. The shaded area indicates events with ΛK^+ mass below 2.2 GeV/c^2, and again shows that the peaks observed in the t_{L0} at this mass (cf. fig. 2) are correlated with the diffractive overlap. In addition, a coherent S_0, P_0 and D_0 superposition with relative magnitude defined by figs. 3a-c yields a $\cos\theta_{GJ}$ distribution which has a sharp forward peak beyond 0.8 and is approximately zero elsewhere, in accord with the diffractive overlap of fig. 4c. Finally, the fit to the low t' distribution shown by the curve in fig. 3d yields mass and width estimates 1870 ± 22 MeV/c^2 and 131 ± 109 MeV/c^2, respectively, for the $\phi_3(1850)$; these values are consistent with those obtained above.

It follows from the above discussion that the $\phi_3(1850)$ is clearly established as an F-wave resonance.

The reason for the difference in the high and low t' distributions of fig. 2 and figs. 3a-d is apparent from fig. 4d. This shows the high t' $\cos\theta_{GJ}$ distribution for the K^-K^+ mass interval 1.84 - 1.88 GeV/c^2. The shaded area indicates events with ΛK^+

mass below 2.2 GeV/c^2. In contrast to fig. 4c, the kinematics of the mapping from the ΔK^+ system to the K^-K^+ system at higher t' causes the diffractive overlap to occur slightly away from the forward direction, thereby creating a forward turnover in the angular distribution. The coherence between the resonant and diffractive amplitudes causes this effect to be maximal near the resonance mass. This results in the high t' dips at this location for t_{40}, t_{50}, t_{60}, and even t_{70} in fig. 2, and in figs. 3b-d. It follows that the observed low t' peaks and high t' dips associated with the helicity zero K^-K^+ amplitudes are both manifestations of the coherence between the F-wave resonance production and the overlapping diffractive ΔK^+ production. The difference in structure is due simply to the t' dependence of the region of overlap in $\cos\theta_{GJ}$.

Projections of the F-wave helicity one contributions are shown in figs. 3e-f, where the low and high t' data have been combined. The signal in fig. 3e comes mostly from the high t' region, and fig. 4b shows that it is not associated with the low mass ΔK^+ region; in fact the signal in fig. 3e corresponds to the faint resonance band observed in the Dalitz plot of fig. 1. The B-W fit yields mass and width estimates of 1852 ± 20 MeV/c^2 and 41 ± 45 MeV/c^2, respectively, and is represented by the curve in fig. 3e; also, the curve in fig. 4b has the same B-W parameters as for fig. 4a, and adequately represents the data. It follows that the high t' resonance parameters, which are obtained from outside the region of diffractive overlap, agree well with those from low t', which are obtained entirely from within the overlap region.

The distribution of fig. 3f is proportional to t_{62}, and has only F-wave contributions. Whereas clear B-W behavior is observed for t_{22} and t_{42} at the $\phi(1020)$ and $f_2'(1525)$, the distribution of fig. 3f appears to oscillate through the resonance region. If, however, the low mass ΔK^+ region is removed, a peak is observed. The oscillatory behavior is associated mainly with the region of diffractive overlap, and indicates that the overlap contributes a relatively real coherent background to the helicity one amplitudes. This

interference effect tends to cancel in the summed contributions of fig. 3e, but the implication is that any F-wave intensity distribution extracted via amplitude analysis will contain background as well as resonance contributions.

Under the assumption of coherence, the number of measured t_{LM} equals the number of unknowns, and an amplitude analysis may be performed by solving the resulting set of quadratic equations. Ambiguities do not significantly affect the solutions for the leading wave, in the present case the F-wave, and so will be discussed no further.

The results of the amplitude analysis are shown in figs. 3g-i. The uncertainties are quite large, since the solutions must describe the values of the eighteen t_{LM} simultaneously in the absence of constraints. Nevertheless, for other than the F_0 distribution at high t', the solutions do peak at ~ 1.86 GeV/c^2. In a simple exchange model, the F_0 intensity at high t' is expected to be less than half that at low t'; the distribution of fig. 4g is bin-by-bin consistent with this, although no peak is observed.

The distributions of total intensity, $|F|^2_{tot}$ ($\equiv |F_0|^2 + |F_-|^2 + |F_+|^2$), shown in fig. 3i, are quite consistent with the t_{00} signals of fig. 2a, and the corresponding combined low and high t' distributions are shown in figs. 5a-b respectively. In fig. 5a, the curve represents the result of the fit to the data of a relativistic F-wave B-W intensity plus a linear background term. This yields

$$M(\phi_3(1850)) = 1855 \pm 22 \text{ MeV/c}^2,$$

$$\Gamma(\phi_3(1850)) = 74 \pm 67 \text{ MeV/c}^2,$$

and we note that this is the first measurement of these parameter values based on an amplitude analysis of the $\phi_3(1850)$ region. The curve of fig. 5b represents the result of a similar fit. This gives an integrated signal which agrees very well with that from fig. 5a, and mass and width estimates of 1851 ± 9 MeV/c^2 and 66 ± 29 MeV/c^2, respectively, in agreement with the results of previous fits to the mass spectrum only [1, 2].

As mentioned previously, a significant $J^P = 3^-$ signal has been obtained in the $\phi_3(1850)$ region from a partial wave analysis of the $K^0_S K^\pm \pi^\mp$ systems using data on reactions (2) from the present experiment [4]. This signal consists solely of $K^*\overline{K}(+c.c.)$ amplitude combinations, and is shown in fig. 5c (open dots) after correction for all unseen decays, including that of the Λ. Also shown are the similarly corrected distribution (solid dots) and curve of fig. 5a. The distribution from reactions (2) is similar in shape to that from reaction (1), and the dashed curve shows the result of a fit to the data using the parameterization of fig. 5a with B-W mass and width fixed at 1855 MeV/c^2 and 74 MeV/c^2, respectively. Integrating the fitted B-W curves over the mass interval 1.72 - 2.04 GeV/c^2, the cross section times branching fraction for the t' range below 1.0 (GeV/c)^2 is measured to be 0.42 ± 0.22 μb for the $K\overline{K}$ mode, and 0.29 ± 0.24 μb for the $(K^*\overline{K} + c.c.)$ mode. The resulting most probable branching ratio value is $BR[(\phi_3(1850) \to (K^*\overline{K} + c.c.))/(\phi_3(1850) \to K\overline{K})] = 0.55^{+0.85}_{-0.45}$, this being obtained from the convolution of the Gaussians representing the cross section estimates. Although the uncertainty is large, this result is consistent with the prediction of Godfrey and Isgur of ~ 0.6 [8]. It is also consistent with the result in ref. 1, although it should be noted that in that paper neither channel was amplitude analysed.

The charged $K\overline{K}$ mass spectrum observed in the reaction $K^-p \to K^-K^0_S\Sigma^+(1385)$ in the present experiment shows no evidence of structure in the $\phi_3(1850)$ region, indicating that its isospin is probably zero.

The $\phi_3(1850)$ is naturally interpreted as the mostly $s\bar{s}$ member of the spin 3 nonet which also includes the $\rho_3(1690)$, the $\omega_3(1670)$, and the $K^*_3(1780)$. Using current mass values [9], a quadratic (linear) mass formula [10] yields an octet-singlet mixing angle of ~ 30° (~ 29°). This indicates that the multiplet is almost ideally mixed, and that the $\phi_3(1850)$ is an almost pure $s\bar{s}$ system, in accord with its production characteristics. The Regge trajectory joining the $\phi(1020)$ and $\phi_3(1850)$ has slope

0.83 ± 0.03 (GeV/c^2)$^{-2}$, intercept 0.13 ± 0.03, and passes slightly above the $f'_2(1525)$; had the $f'_2(1525)$ trajectory the same slope, its first recurrence, the f'_4, would have mass 2176 ± 20 MeV/c^2.

In conclusion, we have presented evidence for the decay of the $\phi_3(1850)$ into $K\overline{K}$ and $K^*\overline{K}(+c.c.)$ final states. Its quantum numbers are $I^G(J^{PC}) = 0^-(3^{--})$, though the evidence for isospin zero is weak, and it is a good candidate to be the mainly $s\bar{s}$ member of the orbitally excited 3^{--} nonet predicted by the quark model.

We are very grateful for the support of the technical staffs of the collaborating institutions.

REFERENCES

1. S. Al-Harran et al., Phys. Lett. 101B (1981) 357.
2. T. Armstrong et al., Phys. Lett. 110B (1982) 77.
3. See, for example, D. Aston et al., SLAC-PUB-4202 / DPNU-87-08 (1987).
4. D. Aston et al., Phys. Lett. 201B (1988) 573.
5. D. Aston et al., The LASS Spectrometer, SLAC-REP-298 (1986).
6. D. Aston et al., DPNU-87-15 / SLAC-PUB-4279 (1987), to be published in Nucl. Phys. B.
7. See, for example, A. Martin et al., Nucl. Phys. B140 (1978) 158.
8. S. Godfrey and N. Isgur, Phys. Rev. D32 (1985) 189.
9. Particle Data Group, Phys. Lett. 170B (1986).
10. M. Gell-Mann, Caltech report TSL-20 (1961) unpublished;
    S. Okubo, Prog. Theor. Phys. 27 (1967) 949.

FIGURE CAPTIONS

1. (a) The Dalitz plot and (b) its K^-K^+ mass projection for reaction (1); (c) the summed $K^0_S K^\pm \pi^\mp$ mass distribution for reactions (2); the data samples correspond to events with $t' \leq 1.0$ (GeV/c)^2.
2. The unnormalized K^-K^+ spherical harmonic moments with $M = 0$ for low (solid dots) and high (open dots) t' in the $\phi_J(1850)$ mass region; the curves in fig. 2a are described in the text.
3. (a)-(f) The mass dependence of particular F-wave contributions to the K^-K^+ angular distribution projected as described in the text; (g)-(i) the F-wave intensity distributions obtained from the amplitude analysis of reaction (1); low and high t' data are denoted by solid and open dots, respectively, while data corresponding to the combined t' range are denoted by crosses; the curves in (a)-(e) are described in the text.
4. (a) The K^-K^+ mass distributions corresponding to ΛK^+ mass below (solid dots) and above (open dots) 2.2 GeV/c^2 in the low t' region; the curve is described in the text; (c) the distribution in K^- t-channel helicity cosine for $1.84 \leq M(K^-K^+) \leq 1.88$ GeV/c^2 at low t'; the shaded area corresponds to ΛK^+ mass below 2.2 GeV/c^2. (b) and (d) As in (a) and (c), but for the high t' region.
5. (a) The total F-wave intensity distribution resulting from the amplitude analysis of reaction (1) for the combined low and high t' regions; (b) the acceptance corrected mass distribution, t_{00}, for the combined low and high t' regions; (c) the comparison of the F-wave intensity distribution of fig. 5a (solid dots) with that obtained from the partial wave analysis of reactions (2) [4] for the $(K^*\overline{K} + c.c.)$ mode (open dots); in each case, corrections have been made for all unseen decay modes, including that of the Λ. The curves in (a)-(c) are described in the text.

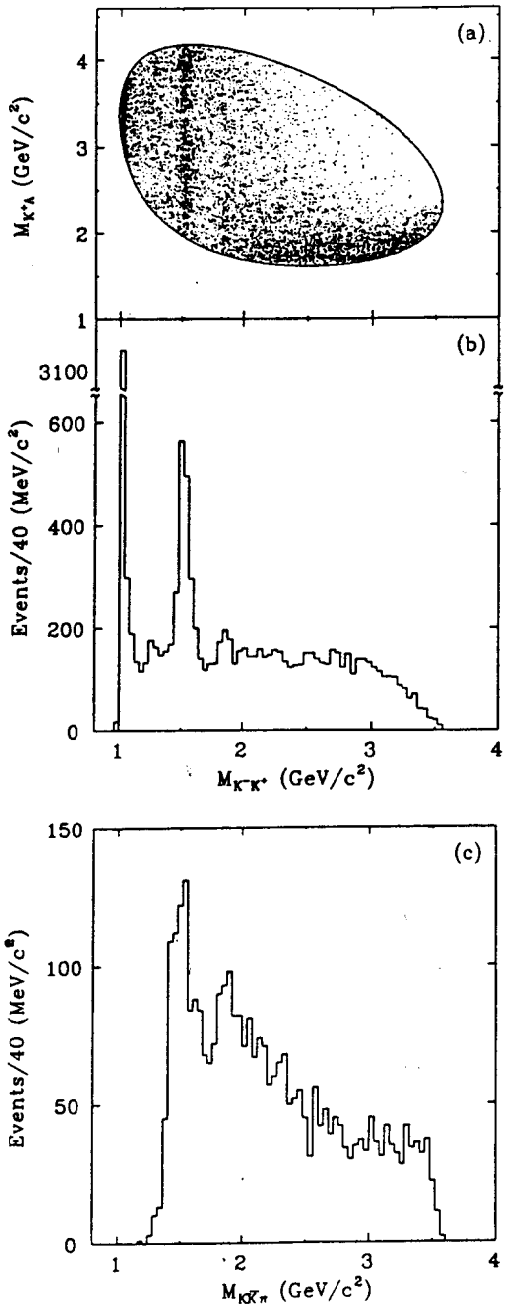
(a)
(b)
(c)
$M_{K^-\Lambda}$ (GeV/c^2)
Events/40 (MeV/c^2)
$M_{K^-K^+}$ (GeV/c^2)
$M_{K\bar{K}\pi}$ (GeV/c^2)

Fig. 1

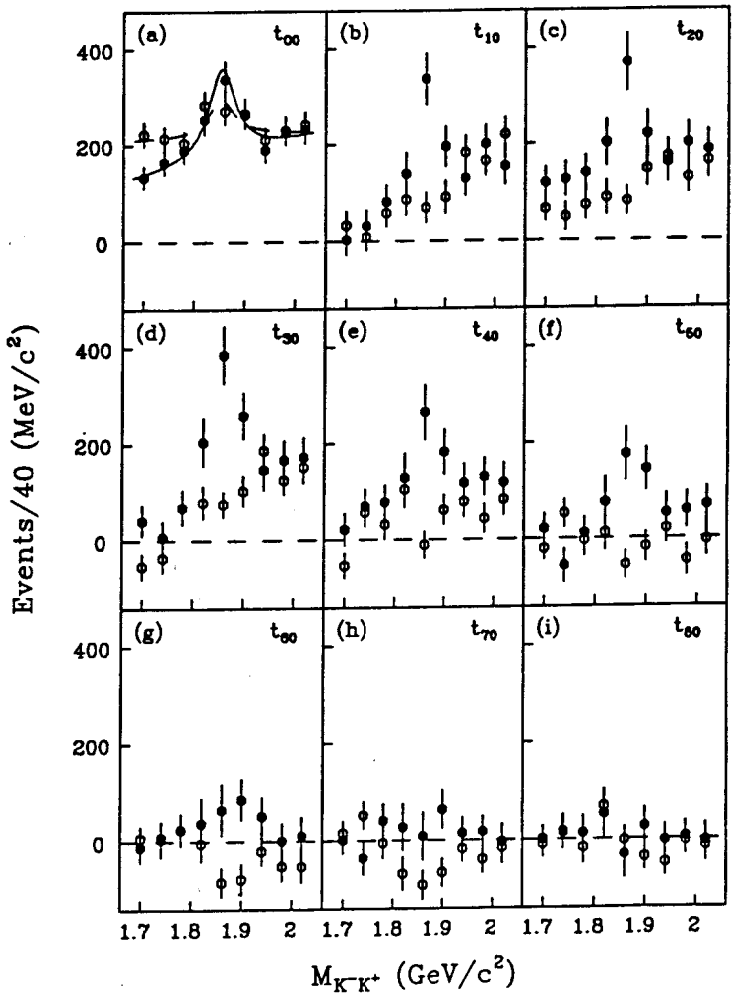
(a) t_{00}
(b) t_{10}
(c) t_{20}
(d) t_{30}
(e) t_{40}
(f) t_{50}
(g) t_{60}
(h) t_{70}
(i) t_{80}
Events/40 (MeV/c^2)
$M_{K^-K^+}$ (GeV/c^2)

Fig. 2

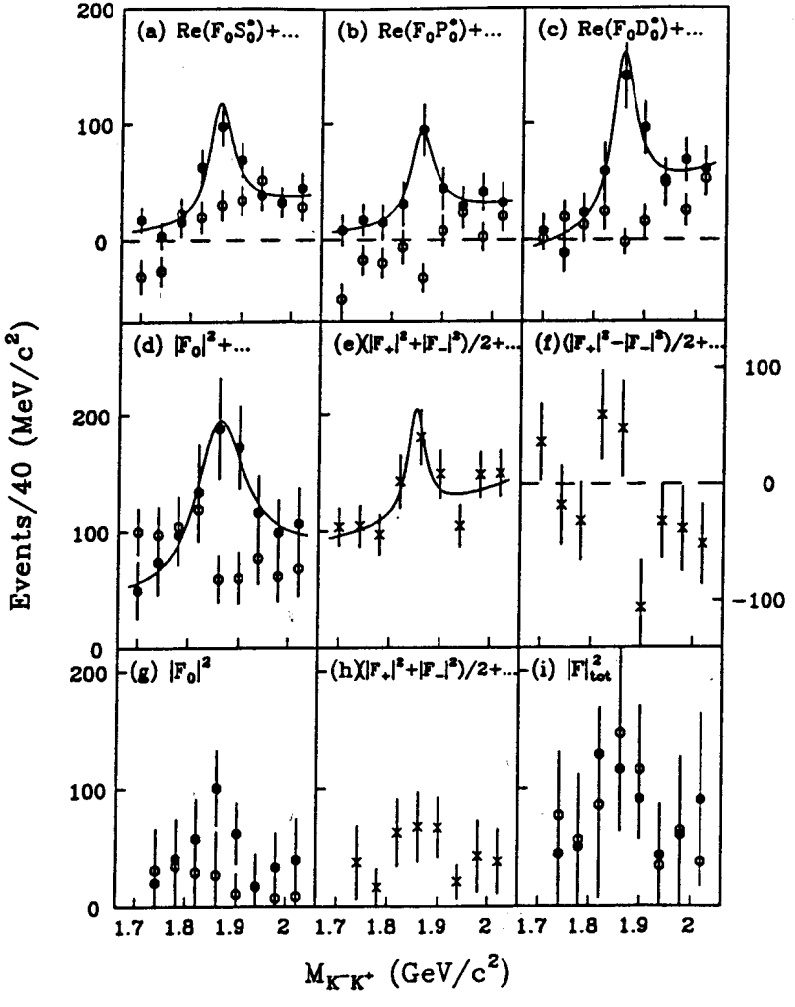
(a) Re($F_0S_0^*$)+...
(b) Re($F_0P_0^*$)+...
(c) Re($F_0D_0^*$)+...
(d) $|F_0|^2$+...
(e)($|F_+|^2$+$|F_-|^2$)/2+...
(f)($|F_+|^2$−$|F_-|^2$)/2+...
(g) $|F_0|^2$
(h)($|F_+|^2$+$|F_-|^2$)/2+...
(i) $|F|^2_{tot}$
Events/40 (MeV/c^2)
$M_{K^-K^+}$ (GeV/c^2)

Fig.3

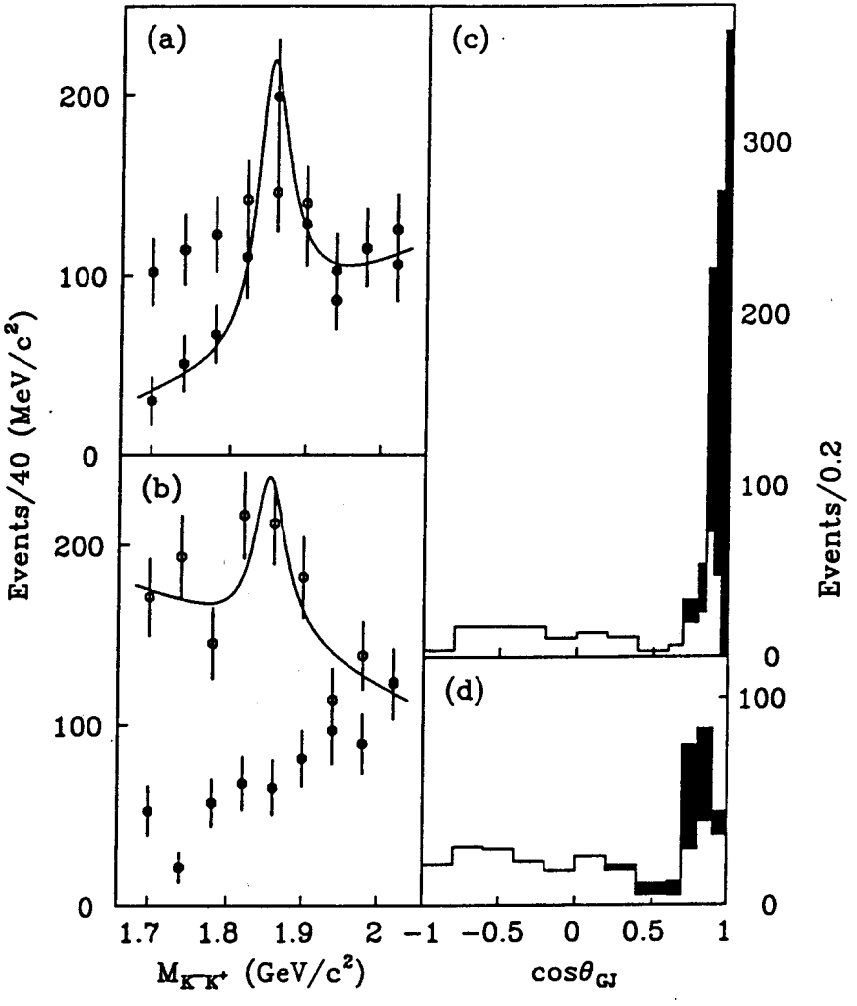
(a)
(b)
(c)
(d)
Events/40 (MeV/c^2)
Events/0.2
$M_{K^-K^+}$ (GeV/c^2)
$\cos\theta_{GJ}$

Fig.4

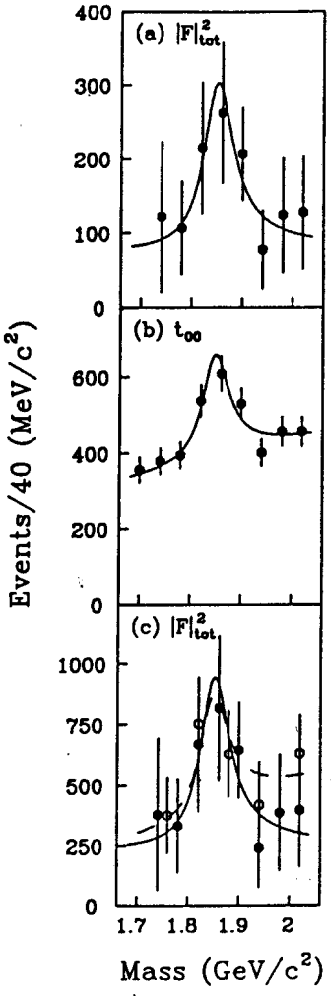
(a) $|F|^2_{tot}$
(b) t_{00}
(c) $|F|^2_{tot}$
Events/40 (MeV/c^2)
Mass (GeV/c^2)
400
300
200
100
0
600
400
200
0
1000
750
500
250
0
1.7
1.8
1.9
2

Fig.5